Ab initio studies of sperrylite, platarsite and palladoarsenide bulk and surface stabilities

B Nemutudi, P P Mkhonto and P E Ngoepe

Materials Modelling Centre, University of Limpopo, Private Bag x1106, Sovenga 0727, South Africa

Email: bradley.nemutudi@ul.ac.za

Abstract. In this study we employed the Vienna *Ab-initio* Simulation Package (VASP) along with the projector augmented wave (PAW) pseudopotential method to investigate the bulk structural and surface stabilities of sperrylite ($PtAs_2$), platarsite (PtAsS) and palladoarsenide (Pd_2As) minerals. The phase stability of PtAsS was obtained using UNiversal CLuster Expansion (UNCLE) code. The phonon dispersion curves showed no soft modes for all the structures, suggesting stability. The calculated surface energies indicated that the (100) surface was the most stable amongst the low Miller index (100), (110) and (111) surfaces for $PtAs_2$, PtAsS and Pd_2As. The order of surface energies increased as: (100) < (111) < (110) for $PtAs_2$ and PtAsS and (100) < (110) < (111) for Pd_2As. The calculated thermodynamically equilibrium morphologies of the relaxed surface structures indicated that the (100) surface was the most dominant for all the studied structures. The findings offer more insight on the stability of these minerals and their surface stability.

1. Introduction

South Africa is one of the leading countries with high percentage of platinum group metal (PGM) in the igneous intrusion of Platreef Bushveld Complex [1]. The most predominant PGMs are platinum (Pt) and palladium (Pd) which consist of about 21% of arsenides [2]. Platinum is extremely resistant to physical and chemical degradation and has exceptional catalytic properties. These properties have led to extensive utilization of jewelry, high temperature industrial and automobile markets [3]. The stability of $PtAs_2$, PtAsS and Pd_2As is important in understanding their mineralogy formation and therefore to their recovery. Furthermore, PGMs which contain both sulphur and arsenide are complex and need a detailed understanding of their stability. First principle calculations have become an important tool for surface scientists as they can determine facet-specific surface energies, surface electronic structures and crystal morphologies [4].

In this paper, we performed density functional theory (DFT) calculations to study structural and vibrational stability of $PtAs_2$, PtAsS and Pd_2As models. The cluster expansion was implemented to generate the platarsite (PtAsS) mix bulk model. The surface calculations were computed to identify the most stable surface (working surface) for $PtAs_2$, PtAsS and Pd_2As minerals. These were complemented with surface morphology in order to identify the preferred plane cleavages.

2. Computational methodology

The bulk and surface stability calculations were performed within the framework of *ab-initio* quantum mechanical density functional theory [5]. The plane-wave (PW) projector augmented wave

pseudopotential with the generalized gradient approximation of Perdew-Burke-Ernzerhof (GGA-PBE) exchange-correlation [6], implemented within the VASP code [7], were employed. The plane-wave cut-off energy was set to 450 and 500 eV for ($PtAs_2$, PtAsS) and Pd_2As bulk models, respectively. The Brillouin zone k-points sampling of 4*4*4 for $PtAs_2$ and PtAsS and 7*7*7 for Pd_2As were used. In the case of surfaces the 4*4*1 for $PtAs_2$ and PtAsS and 5*3*1 for Pd_2As were employed. These were chosen according to the scheme proposed by Monkhorst-Pack [8]. The phonon dispersion spectra were computed using the PHONON code [9]. The interaction range of 10.0 Å for phonon dispersion was used for all the models. These were used to investigate the structural and vibrational properties of $PtAs_2$, PtAsS and Pd_2As minerals. In addition, the UNCLE code within Materials design (MedeA) was performed to generate new stable phase of PtAsS model [10].

To model the surface of the periodic boundary conditions, a slab of finite thickness perpendicular to the surface but infinite extension, i.e. using periodic boundary conditions was used. These slabs surfaces were obtained by cleaving the optimized bulk $PtAs_2$, PtAsS and Pd_2As structures. Slabs were separated from replicas repeating by a vacuum width of 20 Å. Different terminations were tested and only less reactive (low positive surface energy) for (100), (110) and (111) surfaces were considered.

3. Results and discussion

3.1. Cluster expansion and ground state structures of PtAsS model

In order to minimize the sensitivity of the cluster expansion to the user choices, and to make cluster expansion applicable beyond simple binary systems, a new UNCLE program package [11] has been developed. The UNCLE code [12] predicts the ground states of systems containing up to three and more elements. For the cluster expansion method we started by searching for the ground state of the PtAsS system of the DFT energy formation. Our initial starting point was $PtAs_2$, where the sulphur atoms were added automatically by the UNCLE code at the same position as arsenic atoms. The X, Y and Z parameters were also fitted to be equivalent for both As and S atoms. The input methods for the cluster expansion using UNCLE are detailed elsewhere [12].

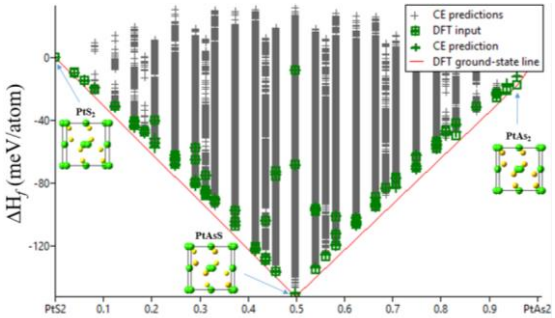

(a)

Iteration	no. of struc.	no. of new struc.	CVS [meV/pos.]	new structures
0	0	2	-	ce1 ce22
0	0	7	-	ce382778 ce1792128 ce25726 ce1675835 ce1859856 ce1 ce22
1	7	5	0.069	ce2902869 ce2010853 ce596364 ce4224 ce6413
2	12	5	0.028	ce6750 ce4149 ce2698233 ce3035270 ce651526
3	17	5	0.0018	ce23 ce10219 ce701620 ce9836 ce270550
4	22	5	0.022	ce711429 ce10211 ce2050374 ce58 ce6234
5	27	5	0.0057	ce3024686 ce710142 ce1827040 ce4319 ce21737
6	32	5	0.86	ce463502 ce428 ce2693643 ce8423 ce3030270
7	37	5	0.69	ce2112830 ce2112096 ce10206 ce2113678 ce704296
8	42	5	0.88	ce166686 ce10190 ce1479445 ce312 ce749341
9	47	5	0.31	ce2847074 ce2868 ce632877 ce723456 ce3035143
10	52	5	1	ce461214 ce24 ce10082 ce18385 ce711426
11	57	5	0.89	ce10185 ce4199 ce70 ce695233 ce2113765
12	62	5	1.1	ce474560 ce4732 ce14304 ce731428 ce759509
13	67	5	1.2	ce3045133 ce2112050 ce711387 ce707467 ce711985
14	72	5	1.2	ce8399 ce632866 ce11964 ce2556 ce1018
15	77	5	1	ce5 ce1644619 ce32 ce2112359 ce526834
16	82	5	1	ce10110 ce53197 ce10191 ce414744 ce3404
17	87	5	1.2	ce4228 ce515032 ce711351 ce2111887 ce4227
18	92	5	1.2	ce710136 ce53213 ce4252 ce711321 ce632546
19	97	5	1.2	ce917 ce8374 ce23863 ce14892 ce18090
20	102	0	1.2	ce917 ce8374 ce23863 ce14892 ce18090

(b)

Pt
As
S

The structures constituting the DFT ground state line, their compositions x and formation energies DHf are:

# x(1:k,1:nC)	DHf / atom [eV]	structure title	cell formula	space group
0.0000000000	1.0000000000	0.0000000000	ce22	Pt4S8	Pa-3
0.5000000000	0.5000000000	-0.1525456250	ce5	Pt4As4S4	P2_13
0.9583333333	0.0416666667	-0.0175684688	ce2111887	Pt12As23S	P3
1.0000000000	0.0000000000	0.0000000000	ce1	Pt4As8	Pa-3

(c)

Figure 1: (a) Shows the cluster expansion diagram obtained in determining the lowest ground states of Pt-As-S structure, (b) shows the iterative obtained stable structures consisting of many pure phases and (c) shows the stable structures that were obtained in the ground state line at x = 0.5.

The binary ground state diagram in Figure 1 shows that all generated structures have negative heat of formation (ΔH_f), hence they are stable. Moreover, the cluster expansion showed a greater stability at 50/50 percentage (x = 0.5) where arsenic and sulphur atoms are equally distributed in the structure with

formed S–As dimer bond at the centre. We found that all structures between PtS_2 and $PtAs_2$, i.e. phases of PtAsS are more stable than PtS_2 and $PtAs_2$ and it was therefore conceivable that a number of phases can form. Moreover, some stoichiometries have multiple DFT inputs and only three of the stable structures of PtS_2, PtAsS and $PtAs_2$ are shown in Figure 1(a). As displayed in Figure 1(b) the last line (i.e. 20th iteration), we can discern that the final cluster expansion contains 102 structures in the training set and has a Cross Validation Score (CVS) of 1.2 meV/pos which is very good for the system. In Figure 1(c) we show the pure phases (Ce1 and Ce22) that possessed the Pa-3 space group, while the mixed phase of PtAsS ($Pt_4As_4S_4$) has P2_13 and P3 space group. We have considered the PtAsS ($Pt_4As_4S_4$) phase with P3 space group as it had a CVS of 1.2 meV/pos and thus preferred phases. This suggested that two stable structures exist on the convex ground state line within the studied concentration range. This revealed that the structure of PtAsS model is quite complex with various stable compounds existing at different arsenic and sulphur concentrations.

3.2. Bulk properties of $PtAs_2$, PtAsS and Pd_2As

The crystal structures of sperrylite (Pa-3 space group), platarsite (P3 space group) are cubic [13] with 12 atoms, while palladoarsenide is monoclinic with space group of P-62m [14] and contain 9 atoms. The full structural relaxations of the bulk models were performed and the calculated structural lattice parameters of the bulk structures are given in Table 1. We found that the lattice constants were in agreement with the experimental data. These comparisons confirm that our computational parameters are reasonably satisfactory and the DFT obtained bulk lattice parameters were in agreement with experiments.

Table 1. The relaxed lattice constants for $PtAs_2$, PtAsS and Pd_2As bulk structures.

Structure	Lattice parameters (Å)	
	Calculated	Experimental
$PtAs_2$	a = b = c = 6.061	a = b = c = 5.970 [15]
PtAsS	a = b = c = 6.024	a = b = c = 5.790 [13]
Pd_2As	a = b = 6.737, c = 3.664	a = b = 6.620, c =3.600 [16]

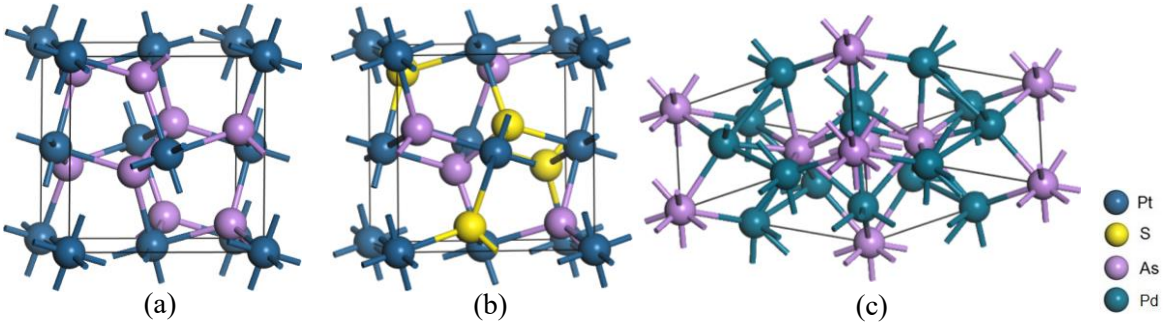

(a) (b) (c)

Figure 2: The relaxed bulk structure: (a) sperrylite ($PtAs_2$), (b) platarsite (PtAsS) and (c) palladoarsenide (Pd_2As).

3.3. Vibrational properties of $PtAs_2$, PtAsS and Pd_2As

The analysis of vibrational properties of $PtAs_2$, PtAsS and Pd_2As phases with respect to the phonon dispersion are shown in Figure 3. The vibrational stability of the structures $PtAs_2$, PtAsS and Pd_2As were carried out along the symmetry directions within the first Brillouin zones.

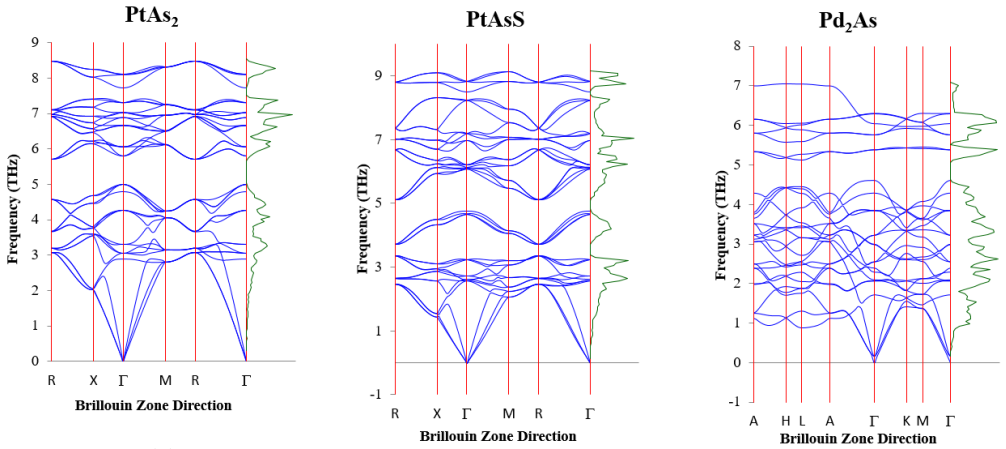

(a) (b) (c)

Figure 3: The phonon dispersion curves: (a) $PtAs_2$, (b) PtAsS and (c) Pd_2As structures.

We observed positive frequencies in all the Brillouin zone directions. As such, our phonon dispersion calculations confirm that $PtAs_2$, PtAsS and Pd_2As structures are vibrationally stable due to the absence of negative vibrations (soft modes) along all directions. However, the PtAsS and Pd_2As system were found to give a scale up to –1 THz, which may suggest a slight overlap of the vibrations to negative. These were ignored and considered as imaginary modes.

3.4. Surface terminations and slab convergence

Considerations must be given to the large number of the Miller index planes (MI), and within each plane, all possible bulk terminations that exist. To reduce the search for working surfaces to a computationally tractable problem, whilst also ensuring that the most likely surfaces were surveyed, we have considered the three low MI planes (100), (110) and (111) terminations that were less reactive (with lowest surface energy) and possessed the bulk terminations. The slab depths were varied as shown in Figure 4(g) for $PtAs_2$ and PtAsS (100) surface and 4(h) for Pd_2As (100) surface. These showed a linear decreasing trend of total energy with an increase in slab thickness. The principal concern is that the slab depth should be sufficient such that both surfaces act as an effectively infinite amount of the bulk solid (i.e. the surfaces do not interact with one another through the solid). Ideally to achieve this, a large slab depth would be required but the computational cost of modelling very deep slabs was avoided. As such the 15-layer slab depth for $PtAs_2$ and PtAsS (100) surface and 21-layers for Pd_2As (100) surface were chosen and considered as thick enough for adsorption.

A supercell surface slab of 2x2 was used for all surfaces for $PtAs_2$, PtAsS and Pd_2As (100) surface. The atomic positions were optimized, where for $PtAs_2$ and PtAsS systems the top two slabs were allowed to relax and the bottom three slabs fixed to the bulk coordinates, while for Pd_2As the top slab was allowed to relax and the bottom two slabs fixed to the bulk coordinates. Figure 4 shows the un-relaxed and relaxed supercell structures for (100) surface of $PtAs_2$, PtAsS and Pd_2As structures. Figure 4(e) showed the slabs that are not identical due to the stacking configuration [17]. The surface stabilities for different terminations were determined from the surface energies using equation 1:

$$E_{surface} = \left(\frac{1}{2A}\right)[E_{slab} - (n_{slab})(E_{bulk})] \quad (1)$$

where E_{slab} is the total energy of the cell containing the surface slab, n_{slab} is the number of atoms in the slab, E_{bulk} is the total energy per atom of the bulk and A is the surface area. A low positive value of $E_{surface}$ indicates stability of the surface termination [3].

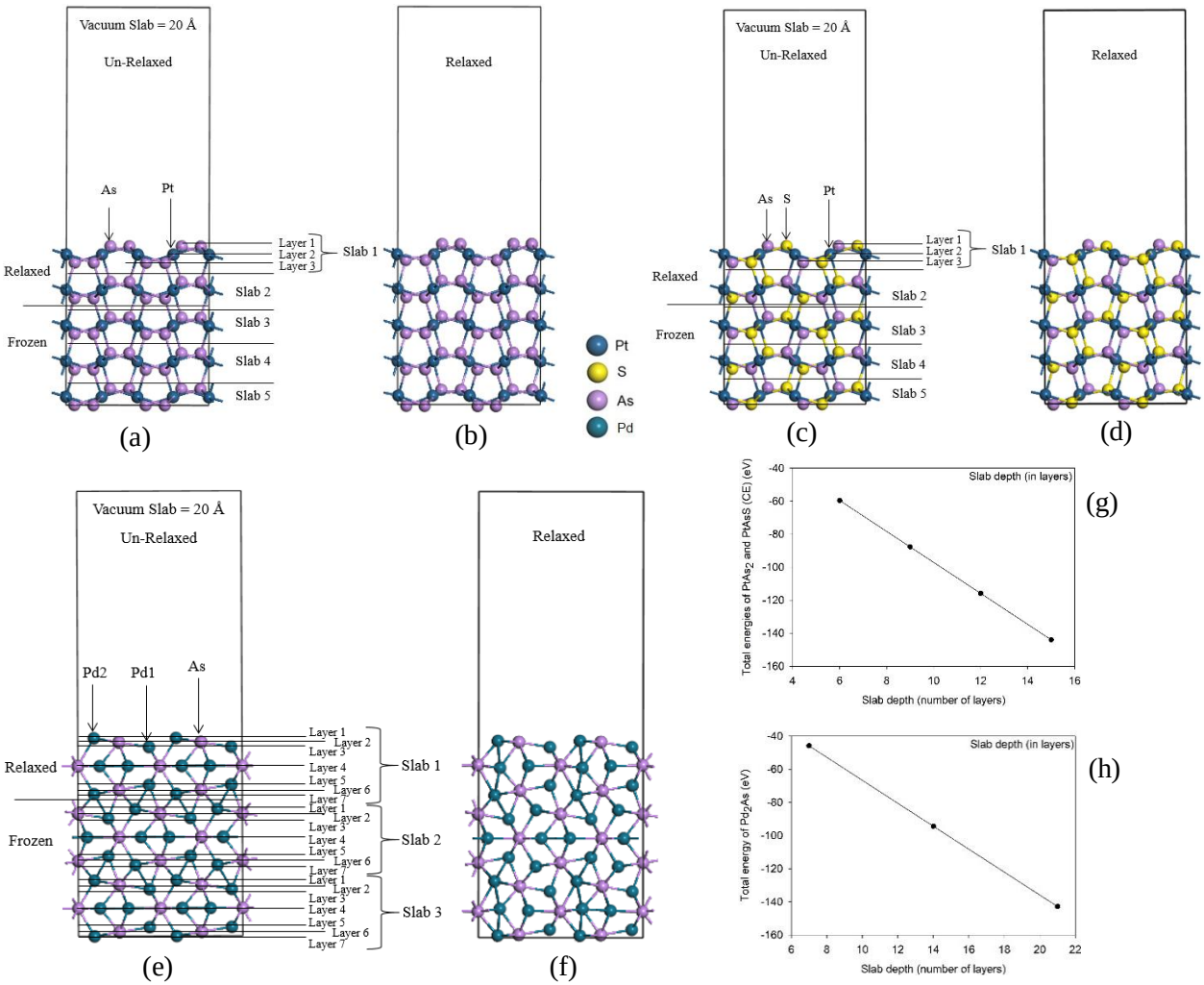

Figure 4: The un-relaxed and relaxed supercell structures of surface layers convergence for (a) and (b) $PtAs_2$, (c) and (d) PtAsS and (e) and (f) Pd_2As (100) surface.

Table 2 shows the supercell surface energies after relaxation for $PtAs_2$, PtAsS and Pd_2AS structures. The computed surface energies increase as: (100) < (111) < (110) for $PtAs_2$ and PtAsS and as (100) < (110) < (111) for Pd_2As. The (100) surface was identified as the most stable surface (working surface) since it displayed the lowest positive energies. Similar working surface for $PtAs_2$ was reported by Waterson et al. [3].

Table 2. The relaxed surface energies for $PtAs_2$ PtAsS and Pd_2As structures.

	Surface energy (eV/Å^2)		
Surface slab	**$PtAs_2$**	**PtAsS**	**Pd_2As**
100	0.065	0.035	0.070
111	0.085	0.062	0.109
110	0.091	0.717	0.097

3.5. Surface morphologies

The crystal morphology of $PtAs_2$, PtAsS and Pd_2As structures were predicted by using calculated surface energies of (100), (110) and (111) surfaces as shown in Table 2 using the METADISE code [17]. The input file for $PtAs_2$ morphology calculation is shown in Figure 5(a). The calculated equilibrium morphologies of the relaxed (100), (110) and (111) surfaces are shown in Figure 5. Our surface

morphologies results indicated that (100) surface was the most dominant surface exposed, followed by (111) and (110) surface for $PtAs_2$ model, with the (110) plane being the smallest. For PtAsS, the surface morphology showed that the mineral preferred to cleave only along the (100) surface plane, since the (110) and (111) surface plane did not appear on the morphology. Furthermore, the (100) surface was the dominant surface exposed on surface morphologies for Pd_2As model. However, in this case the (110) and (111) were also exposed largely, suggesting that these planes may cleave during mineral crushing.

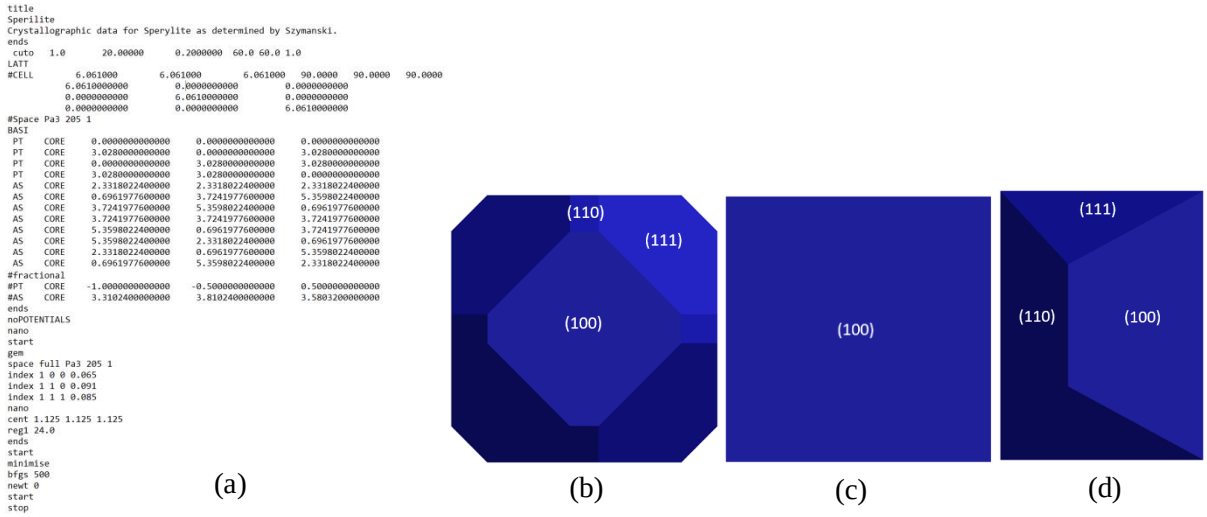

Figure 5: The calculated equilibrium morphologies. (a) Input file for METADISE code to calculate the $PtAs_2$ morphology, (b) $PtAs_2$, (c) PtAsS, and (d) Pd_2As morphologies.

4. Conclusion

In this study, we have performed *ab-initio* DFT calculations to investigate the bulk structural, vibrational and surface properties of $PtAs_2$, PtAsS and Pd_2As minerals. The optimized bulk structural lattice parameters were in agreement with the available experimental values. The phonon dispersion curves showed no soft modes along high symmetry direction suggesting stability for all structures. The PtAsS cluster expansion generated structures were found thermodynamically stable, with the 50:50 (x = 0.5) being the most stable phase. The calculated surface energies indicated that the (100) surface for $PtAs_2$, PtAsS and Pd_2As structures was the most stable amongst the low Miller index (100), (110) and (111). The thermodynamically equilibrium morphologies of the relaxed structures indicated that (100) surface was the most dominant surface. These outcomes gave more insights on the bulk and surface stability of these minerals which demonstrated the preferred plane cleavage of these minerals during mineral grinding.

Acknowledgements

This work was supported and performed at the Materials Modelling Centre (MMC), University of Limpopo. Computing resources were provided by the Centre for High Performance Computing (CHPC). We acknowledge the National Research Foundation (NRF) with a grant number 117587 for financial support.

References

[1] Schouwstra R P, Kinloch E D and Lee C A 2000 Platinum excavation on the UG-2 reef in South Africa *Platinum Met. Rev.* **44** 33–39

[2] Viljoen M J and Schurmann L W 1998 Platinum-group metals *Miner. Resources. S. Afr.* **23** 532–568

[3] Waterson C N, Tasker P A and Morrison C A 2015 Design, synthesis and testing of reagents for high-value mineral collection, Edinburgh: The University of Edinburgh

[4] Manassidis I, De Vita A and Gillan M J 1993 Structure of the (0001) surface of Al_2O_3 from first principles calculations *Surf. Sci. Lett.* **285** 517–521

[5] Hohenberg P and Kohn W 1965 Inhomogeneous electron gas *Phys. Rev.* **136** 864–871

[6] Perdew J, Burke K and Ernzerhof M 1996 Generalized gradient approximation made simple *Phys. Rev. Lett.* **77** 3865–3868

[7] Kresse G and Furthmüller J 1996 Efficient iterative schemes for ab-initio total-energy calculations using a plane-wave basis set *Phys. Rev. B.* **54** 11169–11186

[8] Monkhorst H F and Pack J D 1976 Special points for Brillouin-zone integrations *Phys. Rev. B.* **13** 5188–5192

[9] Parlinski K, Li Z Q and Kawazoe Y 1997 First-principles determination of the soft mode in cubic ZrO_2 *Phys. Rev. Lett.* **78** 4063–4066

[10] Lee R and Raich J 1972 Cluster expansion for solid orthohydrogen *Phys. Rev. B.* **5** 1591–1604

[11] Sanchez J M, Ducastelle F and Gratias D 1984 Generalised cluster description of multicomponent systems *Physica A: Stat. Mech. Appl.* **128** 334–350

[12] Lerch D, Wieckhorst O, Hart G L W, Forcade R W and Muller S 2009 UNCLE: a code for constructing cluster expansions for arbitrary lattices with minimal user-input *Modelling Simul. Mater. Sci. Eng.* **17** 1–19

[13] Cabri L J, Laflamme J H G and Stewart J M 1977 Platinum group minerals from the onverwacht *Can. Mineral.* **15** 385–388

[14] Cabri L J, Laflamme J H G, Stewart J M, Rowland J F and Chen T T 1975 New data on some palladium arsenides and antimonides *Can. Mineral.* **13** 321–335

[15] Ngoepe P E, Ntoahae P S, Mangwenjane S S, Sithole H M, Parker S C, Wright K V and de Leeuw N H 2005 Atomistic simulation studies of iron sulphide, platinum antimonide and platinum arsenide *J. Sci.* **101** 480–483

[16] Olowolafe J O, Ho P S, Hovel H J, Lewis J E and Woodall J M 1979 Contact reactions in Pd/GaAs junctions *J. Appl. Phys.* **50** 955–962

[17] Watson G W, Kesley E T, de Leeuw N H, Harris D J and Parker S C 1996 Atomistic simulation of dislocations, surfaces and interfaces in MgO *J. Chem. Soc. Faraday. Trans.* **92** 433–438